NANO LETTERS

pubs.acs.org/NanoLett Letter

Cellulose Surface Nanoengineering for Visualizing Food Safety

Zewan Lin, Xiaotong Fu, Ke Zheng,* Shaobo Han,* Chaoji Chen, and Dongdong Ye*

Cite This: https://doi.org/10.1021/acs.nanolett.4c01513 Read Online

ACCESS | Metrics & More | Article Recommendations | Supporting Information

ABSTRACT: Food safety is vital to human health, necessitating the development of nondestructive, convenient, and highly sensitive methods for detecting harmful substances. This study integrates cellulose dissolution, aligned regeneration, in situ nanoparticle synthesis, and structural reconstitution to create flexible, transparent, customizable, and nanowrinkled cellulose/Ag nanoparticle membranes (NWCM-Ag). These three-dimensional nanowrinkled structures considerably improve the spatial-electromagnetic-coupling effect of metal nanoparticles on the membrane surface, providing a 2.3×10^8 enhancement factor for the surface-enhanced Raman scattering (SERS) effect for trace detection of pesticides in foods. Notably, the distribution of pesticides in the apple peel and pulp layers is visualized through Raman imaging, confirming that the pesticides penetrate the peel layer into the pulp layer (~30 μm depth). Thus, the risk of pesticide ingestion from fruits cannot be avoided by simple washing other than peeling. This study provides a new idea for designing nanowrinkled structures and broadening cellulose utilization in food safety.

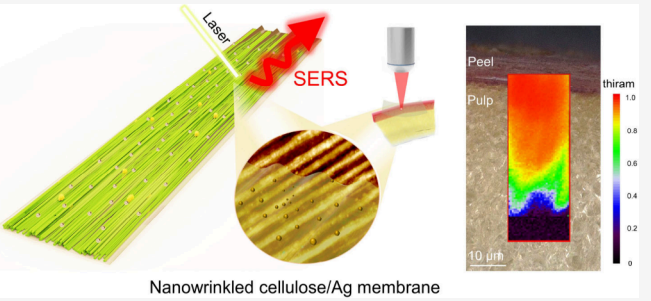

Nanowrinkled cellulose/Ag membrane

KEYWORDS: *cellulose membrane, aligned nanostructure, nanoengineering, Raman imaging, food safety*

In developing countries, food safety, involving microbial and heavy metal contamination, pesticide and veterinary drug residues, excessive use of additives, counterfeiting, and the negative impact of environmental pollution, generally faces severe situations. In addition to measures such as increasing the cost of violating the law and improving the legal system, developing facile, efficient, and visual food safety characterizations is essential. Compared with gas or liquid chromatography, spectroscopic detections, such as Raman spectroscopy (RS) and atomic absorption spectroscopy, are the more widely used nondestructive and convenient analytical techniques in food safety.[1] However, RS is considerably limited by the naturally weak signals generated via inelastic scattering from molecules, making the detection accuracy extremely dependent on the molecular concentration.

Surface-enhanced Raman scattering (SERS)[2] is the most common method that overcomes the aforementioned limitation through near-field coupling of nanoparticles (e.g., Ag,[3] Au,[4] Cu,[5] and TiO_2 nanoparticles[6] and quantum dots[7]) or semiconductor nanosheets (e.g., MXene,[8,9] MoS_2,[10] and graphene[11]) to generate enhanced electromagnetic fields or localized surface plasmon resonances, thereby achieving exponential enhancement of the inelastic scattering signals. Drug compounds,[12,13] water contaminants,[14−16] and metabolites[17,18] have been identified via SERS at quantities below the detection thresholds of RS. SERS research has primarily focused on developing plasmonic nanomaterials,[19,20] designing suitable substrates,[21−23] improving the detection performance,[24] and increasing the flexibility of substrate materials.[25,26]

Flexible substrate materials can better fit irregular detection surfaces than rigid substrates.[27−29] As an environmentally friendly and easily modified biomass material, cellulose is a feasible and flexible template for SERS research.[30−32] Cellulose-based materials, such as paper,[33,34] nanocellulose membranes,[35] cotton fabrics,[36] wet-spun fibers,[37] and cotton swabs,[38] can achieve SERS by depositing or synthesizing functional nanomaterials on the surface. However, such cellulose systems have two characteristics: 1) the transparency and flexibility of the material cannot be balanced, resulting in monotonous detection forms and limited application; 2) the SERS enhancement mechanism only relies on functional nanomaterials, resulting in the weakly SERS-responsive cellulose material.

Herein, we construct a class of regenerated cellulose-composited membranes that integrate transparency (91%), flexibility, and customizable three-dimensional nanowrinkled structures to enhance efficient Raman scattering in complex application scenarios. Unlike traditional isotropic cellulose-based SERS templates[39−41] with a rough or smooth structure, the regenerated-cellulose membranes with aligned, nanowrinkled surface structure fabricated via confined air-drying

Received: March 29, 2024
Revised: July 16, 2024
Accepted: July 19, 2024

https://doi.org/10.1021/acs.nanolett.4c01513
Nano Lett. XXXX, XXX, XXX−XXX

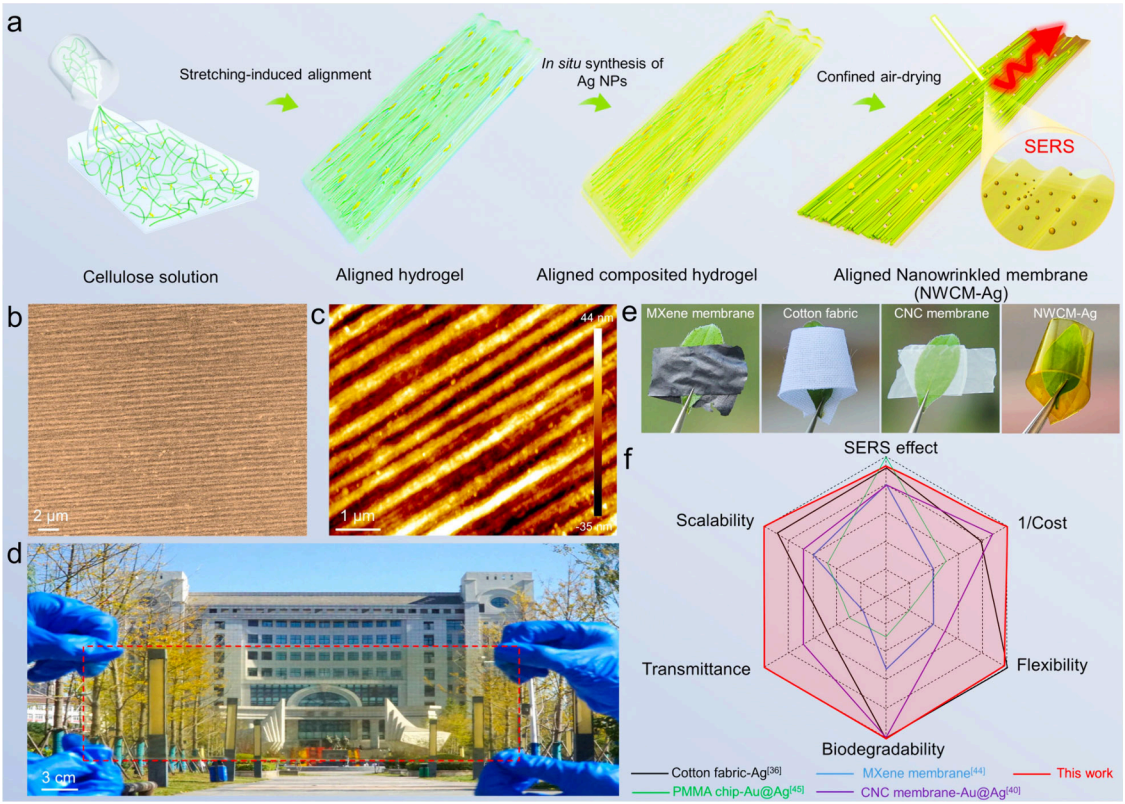

Figure 1. Preparation of the NWCM-Ag membrane. (a) Preparation of NWCM-Ag through confined air-drying of the aligned cellulose hydrogel. The schematic was created by author Zewan Lin through 3D Studio Max software. (b, c) Surface morphologies of NWCM-Ag using SEM and AFM characterizations. (d) Large-scale demonstration of NWCM-Ag. (e) Comparison of light transmittance and flexibility between different membranes. (f) Comprehensive performance analysis of NWCM-Ag based on comparison with representative SERS substrates.

of aligned cellulose hydrogel achieve a three-dimensional distribution of functional nanomaterials on the material surface. A spatially enhanced coupling effect is generated on the surface of membranes, considerably improving the detection performance of the material. Using rhodamine 6G (R6G) and the pesticide thiram as probe molecules, the detection limit was 10^{-9} M, and the enhancement factor reached 2.3×10^{8}. In addition, Raman imaging technology demonstrated spatial detection stability of the composite membrane. Owing to the densification and orientation design of the nanostructure, the composite membranes exhibited excellent mechanical properties and a high SERS performance, enabling efficient detection of additives in food items such as vegetables, fruits, and seafood. The findings of this study provide a reference to further promote flexible SERS materials with a synergistically enhanced microstructure.

Figure 1a and Figure S1 show the process used to prepare NWCM-Ag. Based on our previous study,[42] the regenerated cellulose solution underwent sol−gel transition through covalent cross-linking, and the alkaline gel further formed an aligned cellulose hydrogel comprising a highly oriented nanofibril structure through external force stretching and poor solvent-induced self-aggregation of the cellulose molecular chains. Subsequently, the hydrogel was immersed in silver nitrate and a reducing agent solution sequentially to prepare an aligned composite hydrogel with silver nanoparticles on the surface. Interestingly, unlike the previously reported cellulose membranes with a smooth surface that were air-dried into four-side-confined aligned hydrogels,[43] a three-dimensional nanowrinkle-structured membrane could be constructed by air-drying the two-side-confined aligned cellulose hydrogel along the orientation direction.

The confined-drying strategy endowed NWCM-Ag with a long-range-ordered, parallel-aligned nanowrinkled structure, as confirmed by the SEM and AFM images shown in Figure 1b and 1c, respectively, resulting in a high degree of orientation of NWCM-Ag (Figure S2). Considering that the spot size of the detection laser during RS performed in this study exceeds 250 nm, the adjacent nanowrinkled intervals can be covered entirely by the laser, which provides structural support for applying a three-dimensional nanostructure in SERS detection. Figure 1d shows a large-scale demonstration of NWCM-Ag, which exhibited excellent flexibility to withstand large curvature bending; however, CNC and MXene membranes were brittle (Figure 1e). Furthermore, NWCM-Ag exhibited high optical transmittance, reaching 91% in the visible-light range; the light transmittance at the absorption peak of the Ag nanoparticles was >66% (Figure S3), which indicates the potential to realize transmission Raman detection. To further evaluate the performance of NWCM-Ag, we compared it with other SERS substrates such as a cotton fabric-Ag,[36] an MXene membrane,[44] PMMA chip-Au@Ag,[45] and CNC membrane-Au@Ag.[40] Results showed that NWCM-Ag demonstrated relatively comprehensive and significant performance in terms of the SERS effect, flexibility, transmittance, large-scale fabrication, cost, and stability (Figure 1f; Tables S1−S3).

We further studied the formation process of the surface nanowrinkles of the cellulose hydrogels by monitoring the morphologies of the hydrogel during the confined-drying process. The results demonstrated that the length of the

https://doi.org/10.1021/acs.nanolett.4c01513
Nano Lett. XXXX, XXX, XXX−XXX

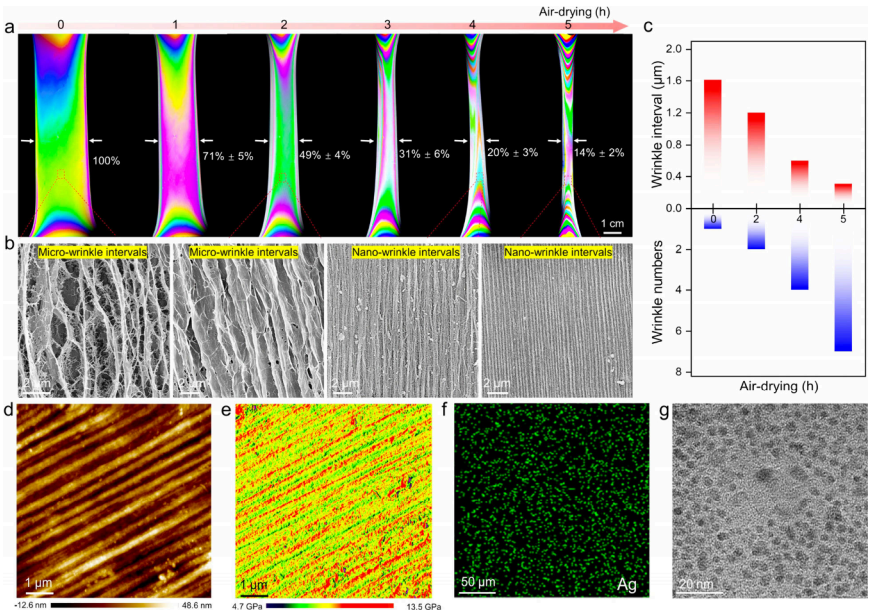

Figure 2. Research on the formation process of nanowrinkles and the characterization of NWCM-Ag. (a) Polarized images of oriented cellulose hydrogels at different drying times. (b) Surface SEM images of cellulose hydrogels during the drying process. (c) Effect of drying time on cellulose nanowrinkle structure. (d) AFM height image and (e) the corresponding Derjaguin−Muller−Toporov (DMT) modulus image of the NWCM-Ag specimen. (f, g) SEM mapping and TEM image of Ag element at the surface of NWCM-Ag.

hydrogel was unchanged along the fixed direction during the drying process, and shrinkage deformation of up to 86% occurred perpendicular to the fixed direction, which was confirmed by bright-field and polarized images (Figure S4 and Figure 2a). In addition, we characterized the morphologies of the hydrogel specimens during the drying process. The results demonstrated that the porous network inside the oriented hydrogel densified gradually (Figure 2b) with the average spacing being reduced from 1.6 to 0.3 μm and the wrinkle density (i.e., the number of wrinkles per 2 μm) increasing from one to seven (Figure 2c), ultimately forming a highly ordered long-range nanowrinkled structure.

Furthermore, we observed that the formation and structural parameters of the nanowrinkles are strongly dependent on the intrinsic structure of the hydrogel. In particular, we found that applying the confined air-drying strategy to the isotropic cellulose hydrogel (λ = 1.0) produced a disordered and nearly smooth surface structure rather than aligned nanowrinkles, as confirmed by the acquired dark polarized image and surface SEM and AFM topography images (Figure S5a). Furthermore, the oriented cellulose membranes obtained after confined air-drying exhibited highly parallel and denser nanowrinkled structures with gradually reduced spacing distances (from 549 to 390 nm) and increased wrinkle density (from three to six) when λ was increased from 1.5 to 2.5 (Figure S5b). The aforementioned results prove that the oriented gel underwent spontaneous shrinkage perpendicular to the orientation direction under restricted drying, thus indicating the possibility of realizing a three-dimensional metal particle distribution.

In fact, the in situ synthesis of silver on the hydrogel surface did not alter the formation of the nanowrinkles during the drying process. For example, the AFM height map of NWCM loaded with Ag nanoparticles demonstrates a periodic parallel nanowrinkled structure (Figure 2d). In addition, we mapped the surface modulus distribution of NWCM-Ag to highlight the distribution of the metal particles on the surface (Figure 2e). Here, by embedding and slicing, we obtained ultrathin samples of the surface structure of NWCM-Ag for transmission electron microscopy (Figure 2g). The results demonstrated that the silver nanoparticles (average size: 20 ± 5.9 nm) were dispersed uniformly on the surface of NWCM-Ag (Figure S6), and the energy-dispersive X-ray spectroscopy image proved that the silver nanoparticles were uniformly loaded on the material surface (Figure 2f). Furthermore, in the representative XRD spectrum of NWCM-Ag, prominent diffraction peaks appeared at 2θ of 37.48°, 43.78°, 64.14°, and 77.3° and were attributed to silver particle (111), (200), (220), and (311) metal crystal plane peaks[46] (Figure S7). In addition, X-ray photoelectron spectroscopy confirmed the valence electron state of the Ag_0 peaks in the membrane, i.e., 373.48 and 367.48 eV for the Ag_{3d} peaks[46] (Figure S8).

Considering that the nanowrinkled structure increases the effective detection area on the cellulose surface irradiated by a single laser spot and endows Ag nanoparticles with a spatial three-dimensional distribution to further enhance the electromagnetic coupling and thereby significantly improve the inelastic scattering signal (Figure 3a), we first tested the Raman spectra of a probe molecule R6G solution (10^{-4} M) impregnated on four types of cellulose membranes, i.e., CM, CM-Ag, NWCM, and NWCM-Ag. The results demonstrated that NWCM-Ag had a much higher enhancement effect than did the other three membranes (Figure 3b). Notably, the NWCM-Ag exhibited more than 11 times the signal enhancement at 1512 cm^{-1} (aromatic C−C stretching of R6G) than CM-Ag (Figure 3c), demonstrating the improvement of the nanowrinkled structure on the SERS effect.

Considering the potential impact of the sparse and dense structure of the nanowrinkled membranes on the SERS effect (Figure S9a), we evaluated the SERS effect of NWCM-Ag for different stretching ratios (i.e., wrinkle densities). As shown in Figure S9b, the SERS effect of the composite membranes for detecting the R6G molecules increased with increasing nanowrinkle density. This may be attributed to the reduced nanowrinkle intervals enlarged by the practical detection areas

https://doi.org/10.1021/acs.nanolett.4c01513
Nano Lett. XXXX, XXX, XXX−XXX

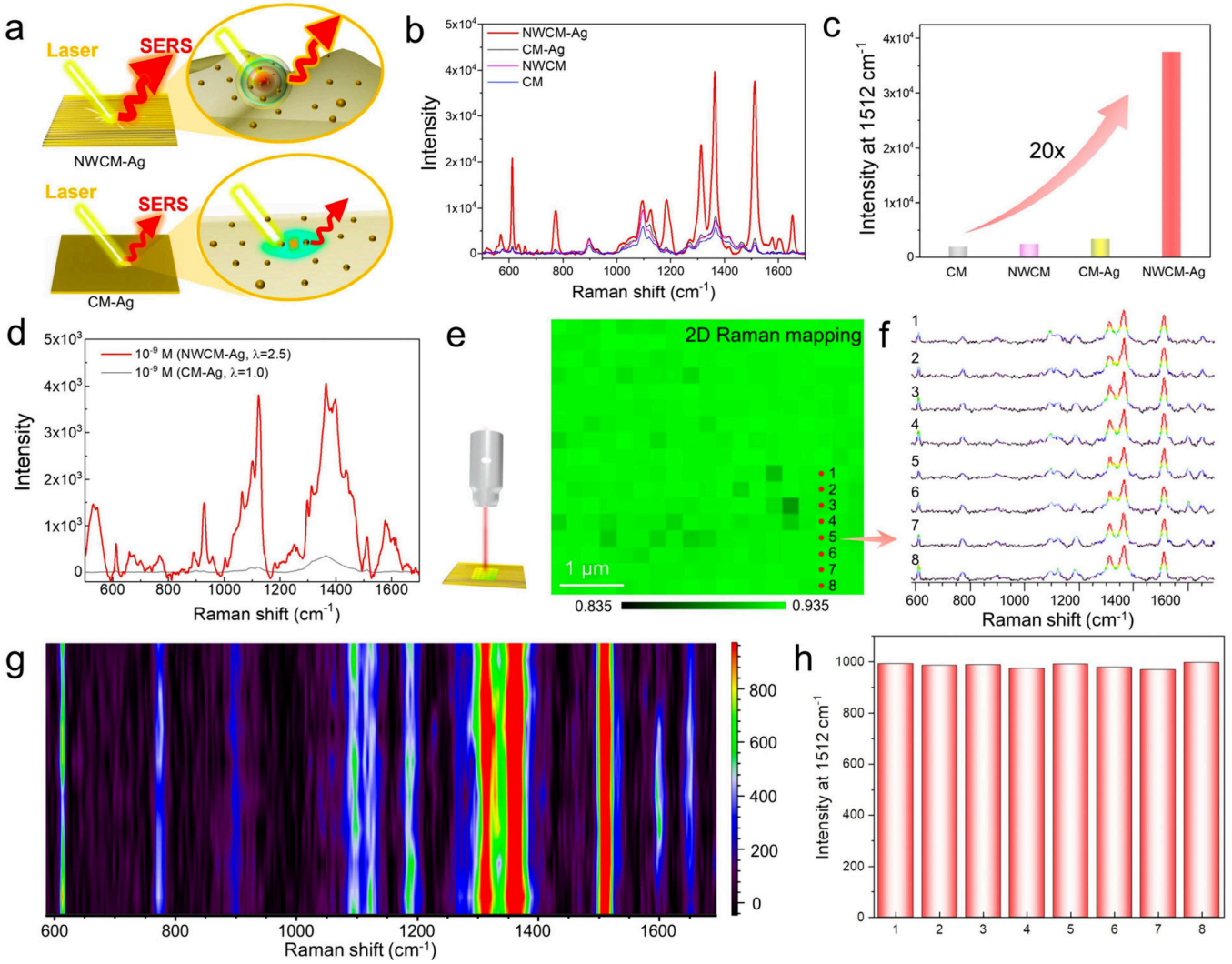

Figure 3. Evaluation of the SERS effect of NWCM-Ag. (a) Schematic diagram of the different SERS effect on smooth and wrinkle structures. (b) Representative Raman spectra of four cellulose membranes against the R6G solution (10^{-4} M) under the same test conditions. (c) Comparison of Raman intensity at 1512 cm^{-1} in four cellulose membranes. (d) Detection capability comparison at ultralow concentrations of NWCM-Ag and CM-Ag. (e) SERS signal uniformity test through plane matrix imaging (19 × 17 points). The representative Raman spectra (f) and the intensity distribution diagram (g) of eight selected adjacent points of testing area. (h) Intensity at 1512 cm^{-1} of the aforementioned Raman spectrum.

on the laser spot irradiation area, thereby strengthening the SERS effect over 60 times (Figure S9c). Even at molecular concentrations as low as 10^{-9} M, high-resolution detection can be achieved using NWCM-Ag (λ = 2.5) (Figure S10). At an ultralow detection concentration of 10^{-9} M, NWCM-Ag (λ = 2.5) demonstrates incredibly higher spectral resolution than CM-Ag (λ = 1.0) (Figure 3d). In addition, absolute enhancement factors (EFs) reaching 2.3×10^8 were calculated as follows by normalizing the intensities for the laser power, acquisition time, and detector sensitivity under the same collection conditions[47,48]

$$EF_S = \frac{I_{SERS}/I_{bulk}}{C_{SERS}/C_{bulk}} \quad (1)$$

where I_{SERS} and I_{bulk} represent the SERS and the conventional Raman intensities at 1365 cm^{-1}, respectively, and C_{SERS} and C_{bulk} represent the concentration of the probe molecules at 10^{-9} and 1 M, respectively.

The uniformity of the substrate's SERS effect is necessary to achieve efficient and stable detection. Raman imaging technology was used to evaluate the detection uniformity of NWCM-Ag for low concentrations of R6G molecules (10^{-9} M). As shown in Figure 3e, 323 points at equal intervals within the test areas exhibited high correlation coefficients, ranging from 0.835 to 0.935, which matched the R6G standard spectrum well and verified the stable identification of the ultralow concentration molecules. In addition, we visualized the intensity distribution three-dimensionally (Figure 3f and 3g) by selecting eight adjacent Raman spectra from the testing area. The overall line shape and characteristic peak intensities exhibited extremely high reproducibility, which proves the uniformity of the SERS effect of subtractions (Figure 3h).

The as-prepared NWCM-Ag integrating light transmittance, flexibility, and the SERS effect has essential applications in food safety detection. For example, pesticides are frequently used during fruit cultivation to increase yields; thus identifying the composition and distribution of pesticides on the surface of and inside fruits is important for protecting human health. In this study, we used the pesticides thiram and CBZ at specific concentrations as models, sprayed them onto the apples'

https://doi.org/10.1021/acs.nanolett.4c01513
Nano Lett. XXXX, XXX, XXX−XXX

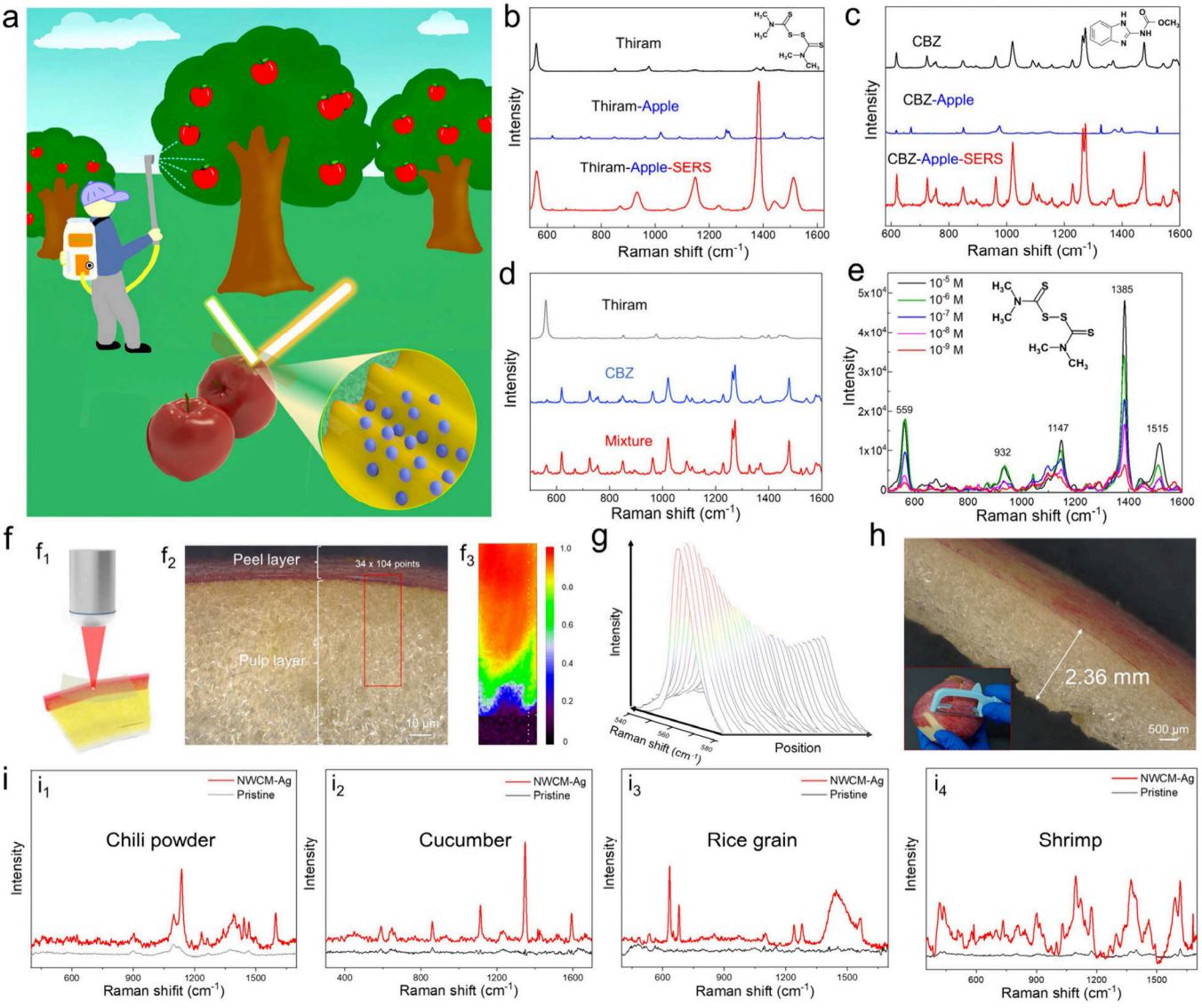

Figure 4. Detection in pesticide and food safety of NWCM-Ag. (a) Schematic diagram of the application of NWCM-Ag in detecting pesticide on apple peel. The schematic was created by author Zewan Lin through Photoshop and 3D Studio Max software. (b, c) Detection of thiram and CBZ on apple peels, respectively, including standards, ordinary tests, and enhanced tests. (d) Enhanced Raman detection of two mixed pesticide spectra. (e) Ultralow concentration detection experiment of thiram on the apple peel surface. (f) Selected 2D Raman imaging (f_1), apple cut section (f_2), and representative Raman spectrum from the peel layer to the pulp layer (f_3). (g) Three-dimensional intensity visualization of thiram at 559 cm^{-1} within the imaging area along the longitudinal axis. (h) Photographs of peeled apples and peel. (i) Universal food testing cases: chili powder (i_1), cucumber (i_2), rice grains (i_3), and shrimp (i_4).

surface, dried them naturally, and then rewashed them to simulate practical scenarios. Subsequently, NWCM-Ag was applied to the apple skin, which was then subjected to Raman testing (Figure 4a). Results demonstrated that, compared with the low-intensity and difficult-to-identify spectra collected without NWCM-Ag (marked as thiram-Apple and CBZ-Apple in Figure 4b and 4c, respectively), the thiram-Apple-SERS and CBZ-Apple-SERS spectra enhanced by NWCM-Ag clearly showed the position of the pesticide characteristic peak and displayed considerably improved photon intensity. In addition, NWCM-Ag can detect complex molecules with high resolution. In other words, the typical Raman spectrum of mixed thiram and CBZ on the surface of the apple peel was identified (Figure 4d). In addition, we evaluated the detection effect after spraying deficient concentrations of pesticides on the peel surface. The results showed that the characteristic Raman spectrum enhanced by the composite membrane could still distinguish the distinct peaks of pesticides even at a thiram concentration as low as 10^{-9} M (Figure 4e), demonstrating the membrane's high sensitivity and SERS effect in practical applications.

Notably, individual cleaning processes and the permeability of pesticides may result in pesticides being present in areas other than the surface of the fruit. Thus, we covered NWCM-Ag on the side section of the apple (including the peel and pulp layers) (Figure 4f_1) and conducted 2D matrix Raman imaging testing on the selected area (Figure 4f_2). The software's built-in algorithm (Wire 5.3, Renishaw) establishes a one-to-one correlation between the test spectrum and the thiram standard spectrum (the index range is 0−1, where 1 means the spectrum is entirely coincident). We obtained a visual distribution image of the pesticide molecules within the

https://doi.org/10.1021/acs.nanolett.4c01513
Nano Lett. XXXX, XXX, XXX−XXX

test range (Figure 4f$_3$). The area near the pericarp layer shows a correlation close to 1, proving that thiram tends to be enriched near the surface layer. In addition, we found that even within the pulp layer, which is approximately 30 μm from the peel, the correlation index still exceeded 0.7. This indicates that the pesticides penetrated the pulp layer and that traditional fruit-cleaning operations cannot wholly remove pesticides. The intensity of the thiram was related to the depth of the pulp layer. In other words, the intensity decreased with increasing depth, indicating a safe depth for pesticide penetration (Figure 4g). Considering that the pulp layer lost during peeling was much larger than 30 μm, which was confirmed by ultradepth-of-field microscopy (Figure 4h), we believe that the peeling operation can effectively avoid the hazards of pesticides in the fruit's epidermis and near-epidermal pulp, thereby reducing the probability of ingesting pesticides. In addition, NWCM-Ag demonstrated enhanced versatility in terms of detecting different types of food (Figure 4i), including condiments (chili powder, Figure 4i$_1$), vegetables (cucumber, Figure 4i$_2$), staple foods (rice, Figure 4i$_3$), and seafood (shrimp, Figure 4i$_4$), which significantly improves the application range of composite membranes in the food security field.

In this study, we developed a process that integrates cellulose dissolution, directional regeneration, nanoparticle synthesis, and nanostructure construction to convert natural cotton linters into customizable NWCM-Ag membranes exhibiting a high SERS performance. The nanowrinkled structure can be tailored in the interval range 549−390 nm by adjusting the degree of orientation and confined air-drying time. Owing to the three-dimensional distribution of metal particles on the surface of the membrane, the effective detection area considerably increases, resulting in an improvement in the electromagnetic coupling performance of the metal particles. NWCM-Ag exhibits a high SERS effect, with the detection limit of R6G reaching 10^{-9} M and an enhancement coefficient of 2.3×10^8, which are sufficient to realize both individual and mixed identification of trace molecules (e.g., 10^{-9} M thiram and CBZ). Furthermore, two-dimensional Raman-enhanced imaging technology was employed to visualize the spatial distribution of pesticides inside the apple. The imaging results prove that the pesticides penetrate the peel layer into the pulp layer (~30 μm). In addition, the NWCM-Ag exhibits a universal SERS effect on various foods, including fruits, vegetables, seafood, condiments, and staple foods, thereby supporting avoiding the intake of harmful substances. The findings of this study provide new concepts for designing cellulose nanostructures and broaden the use of cellulose nanomaterials in SERS applications.

■ ASSOCIATED CONTENT

Supporting Information

The Supporting Information is available free of charge at https://pubs.acs.org/doi/10.1021/acs.nanolett.4c01513.

Additional data on materials characterization, the regulation of nanowrinkled structures, and its measurement of SERS properties (PDF)

■ AUTHOR INFORMATION

Corresponding Authors

Ke Zheng − *School of Materials and Chemistry, Anhui Agricultural University, Hefei 230036, China*; Email: zhengke@ahau.edu.cn

Shaobo Han − *School of Textile Science and Engineering, Wuyi University, Jiangmen 529020, China*; Email: qdhanshaobo@126.com

Dongdong Ye − *School of Materials and Chemistry, Anhui Agricultural University, Hefei 230036, China*; orcid.org/0000-0002-3377-0656; Email: ydd@whu.edu.cn

Authors

Zewan Lin − *School of Materials and Chemistry, Anhui Agricultural University, Hefei 230036, China; School of Textile Science and Engineering, Wuyi University, Jiangmen 529020, China*

Xiaotong Fu − *School of Materials and Chemistry, Anhui Agricultural University, Hefei 230036, China*

Chaoji Chen − *School of Resource and Environment Sciences, Wuhan University, Wuhan 430079, China*; orcid.org/0000-0001-9553-554X

Complete contact information is available at: https://pubs.acs.org/10.1021/acs.nanolett.4c01513

Author Contributions

D.Y. conceived the concept. Z.L. took lead roles in performing the experiments, analyzing data, and drafting the manuscript. X.F. contributed to morphology characterization. D.Y., S.H., and K.Z. provided guidance and support throughout the project. C.C. supervised the aligned nanostructure analysis. All authors contributed intellectually to the study design and approach, discussed the results, and reviewed and edited the final manuscript.

Notes

The authors declare no competing financial interest.

■ ACKNOWLEDGMENTS

This study was supported by the National Natural Science Foundation of China (52103124).

■ REFERENCES

(1) Jiang, G.; Li, Y.; Liu, J.; Liu, L.; Pi, F. Progress on Aptamer-Based SERS Sensors for Food Safety and Quality Assessment: Methodology, Current Applications and Future Trends. *Crit. Rev. Food Sci. Nutr.* **2024**, *64*, 783−800.

(2) Cong, S.; Liu, X.; Jiang, Y.; Zhang, W.; Zhao, Z. Surface Enhanced Raman Scattering Revealed by Interfacial Charge-Transfer Transitions. *Innovation* **2020**, *1*, 100051.

(3) Li, H.; Yin, H.; Dai, H.; Lee, H. K.; Cui, Y.; Sun, F.; Zhang, Y.; An, Q. Enriching Surface-Enhanced Raman Spectral Signatures in Combined Static and Plasmonic Electrical Fields in Self-Powered Substrates. *Nano Energy* **2022**, *92*, 106737.

(4) Li, X.; Zhang, T.; Chen, Z.; Yu, J.; Cao, A.; Liu, D.; Cai, W.; Li, Y. Au Polyhedron Array with Tunable Crystal Facets by PVP-Assisted Thermodynamic Control and Its Sharp Shape As Well As High-Energy Exposed Planes Co-Boosted SERS Activity. *Small* **2022**, *18*, 2105045.

(5) Meng, S.; Liang, J.; Jia, W.; Zhang, P.; Su, Q.; Wang, C.; An, L.; Chen, L.; Wang, Y. Metal-Free and Flexible Surface-Enhanced Raman Scattering Substrate Based on Oxidized Carbon Cloth. *Carbon* **2022**, *189*, 152−161.

(6) Lin, J.; Ren, W. Z.; Li, A. R.; Yao, C. Y.; Chen, T. X.; Ma, X. H.; Wang, X. T.; Wu, A. G. Crystal-Amorphous Core-Shell Structure Synergistically Enabling TiO_2 Nanoparticles' Remarkable SERS Sensitivity for Cancer Cell Imaging. *ACS Appl. Mater. Interfaces* **2020**, *12*, 4204−4211.

(7) Song, G.; Sun, H.; Chen, J.; Chen, Z.; Liu, B.; Liu, Z.; Cong, S.; Zhao, Z. Quantum Effects Enter Semiconductor-Based SERS: Multiresonant $MoO_3{\cdot}xH_2O$ Quantum Dots Enabling Direct, Sensitive

SERS Detection of Small Inorganic Molecules. *Anal. Chem.* **2022**, *94*, 5048−5054.
(8) Jin, J.; Guo, Z.; Fan, D.; Zhao, B. Spotting the Driving Forces for SERS of Two-Dimensional Nanomaterials. *Mater. Horiz.* **2023**, *10*, 1087−1104.
(9) Peng, Y. S.; Lin, C. L.; Long, L.; Masaki, T.; Tang, M.; Yang, L. L.; Liu, J. J.; Huang, Z. R.; Li, Z. Y.; Luo, X. Y.; Lombardi, J. R.; Yang, Y. Charge-Transfer Resonance and Electromagnetic Enhancement Synergistically Enabling MXenes with Excellent SERS Sensitivity for SARS-CoV-2 S Protein Detection. *Nano-Micro Lett.* **2021**, *13*, 52.
(10) Jiang, J.; Liu, H.; Li, X.; Chen, Y.; Gu, C.; Wei, G.; Zhou, J.; Jiang, T. Nonmetallic SERS-Based Immunosensor by Integrating MoS_2 Nanoflower and Nanosheet Towards the Direct Serum Detection of Carbohydrate Antigen 19−9. *Biosens. Bioelectron.* **2021**, *193*, 113481.
(11) Zhang, C.-Y.; Zhao, B.-C.; Hao, R.; Wang, Z.; Hao, Y.-W.; Zhao, B.; Liu, Y.-Q. Graphene Oxide-Highly Anisotropic Noble Metal Hybrid Systems for Intensified Surface Enhanced Raman Scattering and Direct Capture and Sensitive Discrimination in PCBs Monitoring. *J. Hazard. Mater.* **2020**, *385*, 121510.
(12) Riswana Barveen, N.; Wang, T.-J.; Chang, Y.-H. Photochemical Synthesis of Ag/Au/AgCl Heterostructure from Ag Nanowires as A Reusable SERS Substrate for Ultrasensitive Detection of Analgesics and Antibiotics. *Chem. Eng. J.* **2021**, *423*, 130191.
(13) Koike, K.; Bando, K.; Ando, J.; Yamakoshi, H.; Terayama, N.; Dodo, K.; Smith, N. I.; Sodeoka, M.; Fujita, K. Quantitative Drug Dynamics Visualized by Alkyne-Tagged Plasmonic-Enhanced Raman Microscopy. *ACS Nano* **2020**, *14*, 15032−15041.
(14) Tyagi, N.; Sharma, G.; Kumar, D.; Neelratan, P. P.; Sharma, D.; Khanuja, M.; Singh, M. K.; Singh, V.; Kaushik, A.; Sharma, S. K. 2D-MXenes to Tackle Wastewater: From Purification to SERS-Based Sensing. *Coord. Chem. Rev.* **2023**, *496*, 215394.
(15) Han, H.; Song, J.; Hong, J.; Kim, D.; Kang, T. Immiscible Oil−Water Interface: Dual Function of Electrokinetic Concentration of Charged Molecules and Optical Detection with Interfacially Trapped Gold Nanorods. *Anal. Chem.* **2014**, *86*, 6160−6165.
(16) Zhang, Q.; Li, D.; Cao, X.; Gu, H.; Deng, W. Self-Assembled Microgels Arrays for Electrostatic Concentration and Surface-Enhanced Raman Spectroscopy Detection of Charged Pesticides in Seawater. *Anal. Chem.* **2019**, *91*, 11192−11199.
(17) Wang, W.; Kang, S.; Vikesland, P. J. Surface-Enhanced Raman Spectroscopy of Bacterial Metabolites for Bacterial Growth Monitoring and Diagnosis of Viral Infection. *Environ. Sci. Technol.* **2021**, *55*, 9119−9128.
(18) Wang, W.; Chen, Y.; Xiao, C.; Xiao, S.; Wang, C.; Nie, Q.; Xu, P.; Chen, J.; You, R.; Zhang, G.; Lu, Y. Flexible SERS Wearable Sensor Based on Nanocomposite Hydrogel for Detection of Metabolites and PH in Sweat. *Chem. Eng. J.* **2023**, *474*, 145953.
(19) Niu, R.; Gao, F.; Wang, D.; Zhu, D.; Su, S.; Chen, S.; YuWen, L.; Fan, C.; Wang, L.; Chao, J. Pattern Recognition Directed Assembly of Plasmonic Gap Nanostructures for Single-Molecule SERS. *ACS Nano* **2022**, *16*, 14622−14631.
(20) Song, M.; Huang, D.; Huo, N.; Fodjo, E.; Deng, W.; Li, D. Tailoring of Hot Spots in Plasmonic Microgels for Dynamic SERS Detection of Multi-Pesticides by Suction-Release Strategy. *Chem. Eng. J.* **2023**, *473*, 145398.
(21) Banholzer, M. J.; Millstone, J. E.; Qin, L.; Mirkin, C. A. Rationally Designed Nanostructures for Surface-Enhanced Raman Spectroscopy. *Chem. Soc. Rev.* **2008**, *37*, 885.
(22) Das, A.; Pant, U.; Cao, C.; Moirangthem, R. S.; Kamble, H. B. Fabrication of Plasmonic Nanopyramidal Array as Flexible SERS Substrate for Biosensing Application. *Nano Res.* **2023**, *16*, 1132−1140.
(23) Huang, S.; Wu, C.; Wang, Y.; Yang, X.; Yuan, R.; Chai, Y. Ag/TiO_2 Nanocomposites as A Novel SERS Substrate for Construction of Sensitive Biosensor. *Sens. Actuators B Chem.* **2021**, *339*, 129843.
(24) Mohammadi, M.; Antoine, D.; Vitt, M.; Dickie, J. M.; Jyoti, S. S.; Wall, J. G.; Johnson, P. A.; Wawrousek, K. E. A Fast, Ultrasensitive SERS Immunoassay to Detect SARS-CoV-2 in Saliva. *Anal. Chim. Acta* **2022**, *1229*, 340290.
(25) Song, S. W.; Kim, D.; Kim, J.; You, J.; Kim, H. M. Flexible Nanocellulose-Based SERS Substrates for Fast Analysis of Hazardous Materials by Spiral Scanning. *J. Hazard. Mater.* **2021**, *414*, 125160.
(26) Zhang, D.; Pu, H.; Huang, L.; Sun, D.-W. Advances in Flexible Surface-Enhanced Raman Scattering (SERS) Substrates for Non-destructive Food Detection: Fundamentals and Recent Applications. *Trends Food Sci. Technol.* **2021**, *109*, 690−701.
(27) Rostami, S.; Zór, K.; Zhai, D. S.; Viehrig, M.; Morelli, L.; Mehdinia, A.; Smedsgaard, J.; Rindzevicius, T.; Boisen, A. High-Throughput Label-Free Detection of Ochratoxin A in Wine Using Supported Liquid Membrane Extraction and Ag-Capped Silicon Nanopillar SERS Substrates. *Food Control* **2020**, *113*, 107183.
(28) Hu, B.; Pu, H.; Sun, D.-W. Flexible Au@AgNRs/CMC/qPCR Film with Enhanced Sensitivity, Homogeneity, and Stability for In-Situ Extraction and SERS Detection of Thiabendazole on Fruits. *Food Chem.* **2023**, *423*, 135840.
(29) Aleknavičienė, I.; Pabrėža, E.; Talaikis, M.; Jankunec, M.; Račiukaitis, G. Low-Cost SERS Substrate Featuring Laser-Ablated Amorphous Nanostructure. *Appl. Surf. Sci.* **2022**, *571*, 151248.
(30) Hu, B.; Pu, H.; Sun, D.-W. Multifunctional Cellulose-Based Substrates for SERS Smart Sensing: Principles, Applications, and Emerging Trends for Food Safety Detection. *Trends Food Sci. Technol.* **2021**, *110*, 304−320.
(31) Zhang, Q.; Zhang, Y.; Chen, H.; Zhang, L.; Li, P.; Xiao, H.; Wu, W. One-Dimensional Nanohybrids Based on Cellulose Nanocrystals and Their SERS Performance. *Carbohydr. Polym.* **2022**, *284*, 119140.
(32) Lin, Z.; Ye, D. Research progress in structural design of biomass materials aided by Raman imaging technology based on spectral information. *Bas. Sci. J. Text. Univ.* **2024**, *37* (3), 1−10.
(33) Huang, C.-C.; Cheng, C.-Y.; Lai, Y.-S. Paper-Based Flexible Surface Enhanced Raman Scattering Platforms and Their Applications to Food Safety. *Trends Food Sci. Technol.* **2020**, *100*, 349−358.
(34) Wu, L.; Zhang, W.; Liu, C.; Foda, M. F.; Zhu, Y. Strawberry-Like SiO_2/Ag Nanocomposites Immersed Filter Paper as SERS Substrate for Acrylamide Detection. *Food Chem.* **2020**, *328*, 127106.
(35) Marques, A. C.; Pinheiro, T.; Morais, M.; Martins, C.; Andrade, A. F.; Martins, R.; Sales, M. G. F.; Fortunato, E. Bottom-Up Microwave-Assisted Seed-Mediated Synthesis of Gold Nanoparticles onto Nanocellulose to Boost Stability and High Performance for SERS Applications. *Appl. Surf. Sci.* **2021**, *561*, 150060.
(36) Gao, W.; Xu, J.; Cheng, C.; Qiu, S.; Jiang, S. Rapid and Highly Sensitive SERS Detection of Fungicide Based on Flexible "Wash Free" Metallic Textile. *Appl. Surf. Sci.* **2020**, *512*, 144693.
(37) Skwierczyńska, M.; Woźny, P.; Runowski, M.; Kulpiński, P.; Lis, S. Optically Active Plasmonic Cellulose Fibers Based on Au Nanorods for SERS Applications. *Carbohydr. Polym.* **2022**, *279*, 119010.
(38) Huang, W.-C.; Chen, H.-R. Application of Cotton Swab−Ag Composite as Flexible Surface-Enhanced Raman Scattering Substrate for DMMP Detection. *Molecules* **2023**, *28*, 520.
(39) Xian, L.; You, R. Y.; Lu, D. C.; Wu, C. J.; Feng, S. Y.; Lu, Y. D. Surface-Modified Paper-Based SERS Substrates for Direct-Droplet Quantitative Determination of Trace Substances. *Cellulose* **2020**, *27*, 1483−1495.
(40) Wu, J.; Xi, J.; Chen, H.; Li, S.; Zhang, L.; Li, P.; Wu, W. Flexible 2D Nanocellulose-Based SERS Substrate for Pesticide Residue Detection. *Carbohydr. Polym.* **2022**, *277*, 118890.
(41) Cheng, D.; He, M.; Ran, J.; Cai, G.; Wu, J.; Wang, X. Depositing a Flexible Substrate of Triangular Silver Nanoplates onto Cotton Fabrics for Sensitive SERS Detection. *Sens. Actuators B Chem.* **2018**, *270*, 508−517.
(42) Ye, D.; Yang, P.; Lei, X.; Zhang, D.; Li, L.; Chang, C.; Sun, P.; Zhang, L. Robust Anisotropic Cellulose Hydrogels Fabricated via Strong Self-Aggregation Forces for Cardiomyocytes Unidirectional Growth. *Chem. Mater.* **2018**, *30*, 5175−5183.

https://doi.org/10.1021/acs.nanolett.4c01513
Nano Lett. XXXX, XXX, XXX−XXX

(43) Ye, D.; Lei, X.; Li, T.; Cheng, Q.; Chang, C.; Hu, L.; Zhang, L. Ultrahigh Tough, Super Clear, and Highly Anisotropic Nanofiber-Structured Regenerated Cellulose Films. *ACS Nano* **2019**, *13*, 4843−4853.
(44) Limbu, T. B.; Chitara, B.; Orlando, J. D.; Garcia Cervantes, M. Y.; Kumari, S.; Li, Q.; Tang, Y.; Yan, F. Green Synthesis of Reduced $Ti_3C_2T_x$ MXene Nanosheets with Enhanced Conductivity, Oxidation Stability, and SERS Activity. *J. Mater. Chem. C* **2020**, *8*, 4722−4731.
(45) Yan, S.; Sun, J.; Chen, B.; Wang, L.; Bian, S.; Sawan, M.; Tang, H.; Wen, L.; Meng, G. Manipulating Coupled Field Enhancement in Slot-under-Groove Nanoarrays for Universal Surface-Enhanced Raman Scattering. *ACS Nano* **2023**, *17*, 22766.
(46) Ye, D.; Zhong, Z. B.; Xu, H.; Chang, C. Y.; Yang, Z. X.; Wang, Y. F.; Ye, Q. F.; Zhang, L. N. Construction of Cellulose/Nanosilver Sponge Materials and Their Antibacterial Activities for Infected Wounds Healing. *Cellulose* **2016**, *23*, 749−763.
(47) Le Ru, E. C.; Blackie, E.; Meyer, M.; Etchegoin, P. G. Surface Enhanced Raman Scattering Enhancement Factors: A Comprehensive Study. *J. Phys. Chem. C* **2007**, *111*, 13794−13803.
(48) Cai, W. B.; Ren, B.; Li, X. Q.; She, C. X.; Liu, F. M.; Cai, X. W.; Tian, Z. Q. Investigation of Surface-Enhanced Raman Scattering from Platinum Electrodes Using a Confocal Raman Microscope: Dependence of Surface Roughening Pretreatment. *Surf. Sci.* **1998**, *406*, 9−22.

https://doi.org/10.1021/acs.nanolett.4c01513
Nano Lett. XXXX, XXX, XXX−XXX